Variation of crystallinity of Cu and Cu$_2$O nanowires arrays grown in various pores of porous alumina membrane

Yu-Min Shen[1], Wen-Fang Chiu[1], Sheng-Chang Wang[2], Pramoda K. Nayak[1], Dipti. R. Sahu[1, 3*] and Jow-Lay Huang[1, 4, 5*]

[1]*Department of Materials Science and Engineering, National Cheng Kung University, Tainan 701, Taiwan, Republic of China*
[2]*Department of Mechanical Engineering, Southern Taiwan University of Science and Technology, Tainan 710, Taiwan, Republic of China*
[3]*Department of Natural and Applied Sciences, Namibia University of Science and Technology, Private Bag 13388, Windhoek, Namibia*
[4]*Center for Micro/Nano Science and Technology, National Cheng Kung University, Tainan 701, Taiwan, Republic of China*
[5]*Research Center for Energy Technology and Strategy, National Cheng Kung University, Tainan 701, Taiwan, Republic of China*

*Corresponding author, Tel: +264-61-2072783, +886-6-234818, Fax: +264-61-2079783;
E-mail: dsahu@nust.na, jlh888@mail.ncku.edu.tw

Abstract

Various pore sizes of a porous alumina membrane were fabricated using H$_2$SO$_4$ and H$_2$C$_2$O$_4$ electrolyte under different ionization voltages. Cu nanowire arrays with high aspect ratios, uniform pore size, and ordered pore arrangement were synthesized using the above porous alumina membrane (PAM). Moreover, Cu$_2$O nanowire arrays were prepared through the oxidization of Cu metal nanowire arrays. From the microstructure and compositional analysis, it was observed that pores of different sizes, i.e. 20~30, 70~90 and 90~100 nm could be obtained by controlling various electrolytes and anodization voltage. The Cu nanowire synthesized with various pore sizes were found to be single crystal (20~90 nm) and polycrystalline (90~100nm) respectively. The single crystal Cu with (111) direction was occurred due to homogeneous current density distribution and relationship between current density (J) and nucleus radius (r$_o$). After oxidation of Cu, the Cu$_2$O nanowires with the pore sizes of 20~100 nm was found to be single crystal. The rearranged of Cu and O$_2$ lattice sites promotes the enhancement of crystalline property. Copyright © 2017 VBRI Press.

Keywords: Nanowires, PAM, anodization, crystallinity, Cu$_2$O.

Introduction

There are many intensive studies on nanostructure materials such as nanotubes, nanowires, nanosprings and nanorods for their unique electrical, chemical, optical, mechanical, sensing, and magnetic properties for possible applications in nanodevices [1-4]. The fabrication of different nanostructure using unique and innovative method is the interest of researcher worldwide to get specific nanostructure for specific application. Template synthesis is a one of the bottom-up technology widely applied to fabricate various kinds of nanostructure, especially nanoparticles, nanotubes, and nanowires. A well-known template called porous alumina membrane (PAM), featuring order pore arrays, narrow size distribution, and high aspect ratios [5], has attracted much attention for the synthesis of 1-D nanostructures [6,7]. PAM having pore size 30nm to few hundred are

synthesized depending on the processing electrolyte and voltage [8-9] for different applications. In addition, much work has been devoted for synthesizing metal [10-12] and metal oxide nanowire arrays directly from PAM template [13-17]. PAM having better characteristics such as tunable pore size, uniform structure and high thermal stability become the most interesting material in nanofabrication.

The growth of metal and metal oxide nanowires directly from PAM plays important role for potential applications in devices [18]. A significant level of control over the growth of nanowires on PAM is necessary for the fabrication of devices. The crystallinity of metal and metal oxide nanowires plays unique role for this applications. Now Cu and Cu$_2$O nanowires has emerged great attention due to its superior characteristics and applications [19-21]. However, the stability of Cu

nanowires against oxygen, high temperatures, and chemical etching makes difficult for large scalable fabrication, before Cu nanowires can be fully integrated into commercial devices. The challenges remain also for the stabilization of Cu nanowires because they are prone to oxidation under ambient conditions. As a result, the growth of Cu and Cu_xO nanowires is more important for future applications. Cu are single crystal under low deposition potential and polycrystalline under high deposition potential. Polycrystalline Cu_2O nanowire array growth via PAM was studied using three-electrode electrochemical deposition [22-25]. Oh et al. [22] fabricated Cu_2O-based nanowires on PAM using aqueous $CuSO_4$ and lactic acid solutions with a pH = 9. Choi et al. [23] observed that nanowire arrays of Cu reduced into Cu_2O when the pH was changed from 6 to 10. Inguanta et al. [24] synthesized Cu_2O nanowire arrays at 55ºC with pH=6.5 and -0.2V vs. SCE (saturated calomel electrode) in copper acetate and sodium acetate solutions. They also explored the different potential form on pulse to avoid the co-deposition of Cu and Cu_2O [25].

Many researchers have focused on the direct synthesis of Cu_2O nanowire arrays by the electrochemical process; however, the prepared Cu_2O nanowires were found to be polycrystalline in nature. The growth mechanism of Cu_2O nanowires on PAMs is assumed to occur through particle agglomeration in the nano channels. It has been proposed that single crystal nanowires or nanorods provide direct paths for transporting electrons, with the electron transport rate in single crystals being several orders greater than that of their polycrystalline counterpart [26]. Hence, fabricating single crystals nanowire is paramount for improving electrical properties. In this regard, Xu et. al [27] reported the synthesis of CdS nanowire by controlling the pore size of PAMs under electrochemical deposition method. Ultimately, they observed single crystal CdS nanowires with a pore size diameter close to 8 nm. Single crystal CdS growth was achieved via atom-by-atom assembly of individual crystallites instead of the agglomeration of particles formed in the solution phase. Furthermore, in our previous work [28], we have synthesized Cu_2O nanowire arrays by annealing Cu/PAMs composition under various partial oxygen atmospheres. Present work report the possibility of synthesis of Cu nanowire arrays by controlling the pore size of PAMs using electrochemical deposition and Cu_2O single nanowires by heating the Cu/PAMs nanowires than those reported in the literature so far. The crystallinity of the nanowires is controlled depending on the size of the pore. The synthesized Cu nanowires may have potential application in devices such as electrostatic dissipative and current collector for batteries of Li and Cu_2O can be a candidate for use in next generation memory devices.

Experimental

Preparation of porous alumina membranes (PAMs)

PAMs was prepared using the well-known procedure using Al foil with anodization process as described elsewhere [16]. The Al foil sheet were annealed, cleaned and finally electro polished in a mixture of $HClO_4$-C_2H_5OH (1:4 vol %) at 10ºC, with a current density of $100mA/cm^2$ for 1 min.

The standard anodization was carried out in 0.3 M sulfuric acid and 0.3 M oxalic acid at a constant voltage of 18, 40 and 60V using Pt foil as the counter electrode. The electrolyte was then vigorously stirred, with a temperature kept at 0ºC during anodization. After 3~6 h of anodization, the alumina film was selectively etched away in a mixture of H_3PO_4- CrO_3-H_2O (2g-3.5 mL-100 mL) at 70ºC for 40 min. Afterwards, the film underwent a second anodization process under the same conditions for 18~24 h. After the second anodization, the remaining Al was dissolved by saturated $HgCl_2$ solution. Finally, the straight nano channel pores were handled by dissolving the barrier layer with 5% H_3PO_4 solution at 60ºC for 20 min.

Preparation of Cu/PAMs and Cu₂O/PAMs nanowires arrays

A layer of Ti (10 nm) and Pt (100 nm) were coated onto one side of the membrane before deposition of nanowire arrays and adhered to the Cu substrate to serve as the working electrode (cathode). Pt foil (anode) and a saturated calomel electrode (SCE, 0.241V/NHE) served as the counter and reference electrodes, respectively, in a three-electrode electrochemical deposition system. A potentiostat (263A, Princeton Applied Research) was used to provide potential and also to record the current density-time (J-t) curve during fabrication of the Cu nanowire. The PAMs/Ti/Pt/Cu were degassed using a mixture of 0.2 M $CuSO_4$ and 0.15 M H_3BO_3 solution with a pH = 2 (controlled by H_2SO_4) and deposited at -0.18 V/SCE for 2 h. After electrochemical deposition, the Cu/PAMs nanowire arrays were annealed in air at 400ºC for 8 h to obtain the Cu_2O/PAMs nanowire arrays.

Characterization of Cu/PAMs and Cu₂O/PAMs nanowires arrays

The microstructure and chemical composition of the prepared Cu and Cu_2O nanowire arrays were analyzed by employing field emission scanning electron microscopy (FE-SEM), high resolution transmission electron microscopy (HR-TEM), and an energy dispersive spectrometer (EDS). For SEM observation, Cu/PAMs and Cu_2O/PAMs were immersed in a 1M NaOH solution for 30 min, and then cleaned by deionized water several times. The HR-TEM samples were prepared by immersing the Cu/PAMs and Cu_2O/PAMs in 3M NaOH for 5 min, and then washed by deionized water several times. The same step was repeated 3 times until the Cu/PAMs and Cu_2O/PAMs became soft. Subsequently, the samples were dispersed in ethanol and collected onto the Ni grid.

Results and discussion

The various pore sizes of PAMs were prepared using sulfuric acid and oxalic acid under 18 V to 60 V anodization voltages. Many experimental parameters such as electrolyte concentration, the anodic voltage, anodic

time, formation temperature, oxidation time, annealing temperature and etching process are used to get the required pore size of PAM [10]. The size of the pore can be easily controlled by changing the processing condition. **Fig. 1** shows the SEM top-view morphology of PAM prepared under different conditions, which consists of uniform pore arrays. The pore size distribution of PAM using sulfuric acid at 18 V was around 20-40 nm (**Fig. 1A**). Using oxalic acid, the average pore size for anodization voltages of 40 V to 60 V was around 70~90 and 90~100 nm respectively (Figs. 1B-C). According to Lee et. al **[29],** the pore size distribution with respect to voltage exhibits a linear relationship in a mild anodization (MA) process, which is consistent with our results. Pore size of PAM is crucial for growth of nanostructure.
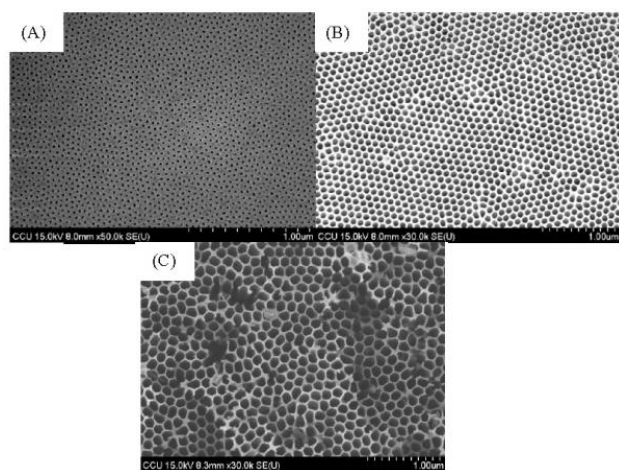
Fig. 1. SEM images of PAM template under (A) H$_2$SO$_4$ solution, 18 V, and H$_2$C$_2$O$_4$ solution (B) 40 V and (C) 60 V.
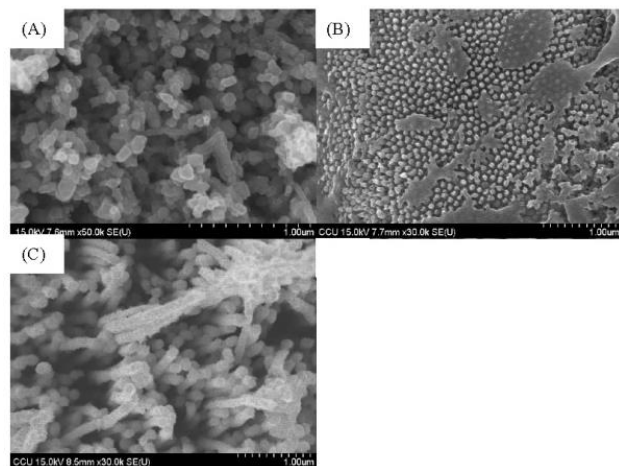
Fig. 2. Plane-view SEM images of Cu nanowire arrays with diameter equal to various PAM pore sizes (A) 20~30, (B) 70~90 and (C) 90~100. PAMs were removed using 1 M NaOH solution for 30 min.

Since the various pore sizes of PAMs were obtained by controlling the electrolyte and anodization voltage, the Cu nanowires were embedded into the nano channel of PAMs using electrochemical deposition. **Fig. 2** shows that the Cu nanowire arrays, which were initially embedded in various pore sizes of PAM, and became free standing after the PAMs were removed using a NaOH solution. As

much, the size and arrangement of nanowires depend on the PAMs and pore sizes were found to be around 20-40, 70-90 and 90-100 nm respectively. The crystallinity of individual nanowires was investigated via TEM images, as shown in **Fig. 3.** Initially, to confirm the size of each nanowire, observed diameters measured 30, 70, and 90 nm (**Figs. 3 A, C and E),** which was similar to the SEM results. It can be seen that the nanowire shape and size were controlled directly by the template. The electron diffraction patterns show single crystal formations when the nanowire was fabricated with diameters of 20-40 and 70-90 nm. When the nanowire increased to 90 nm, a fibrillar structure was observed, and the nanowire crystallinity was polycrystalline (as shown in **Fig 3F.** Further, the d-spacing is found to be 2.43 Å, and the growth direction is along (111). The prefer orientation of Cu was (111) due to the lowest surface energy during growth process.
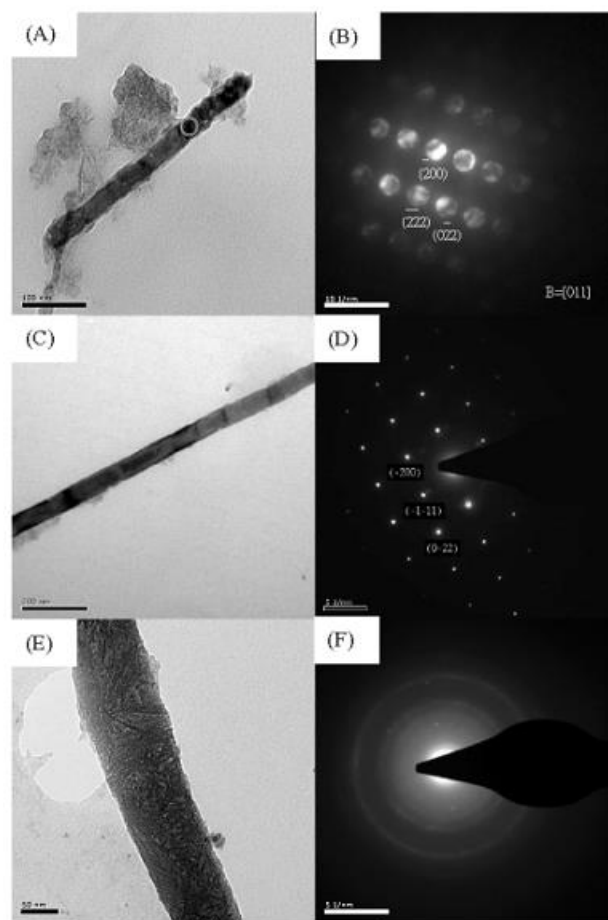
Fig. 3. TEM and ED images of Cu nanowire arrays with diameters of (A, B) 20~30, (C, D) 70~90 and (E, F) 90~100 nm

To determine the Cu nanowire growth rate under various PAM pore sizes, the J-t curve at a constant potential of -0.18 V/SCE was plotted and shown in **Fig. 4**. Generally, synthesis of nanowire by template assistance consists of three steps, which are shown in **Fig. 4A**. In the first step, Cu_{aq}^{2+} migrates to the interface of the electrode (Pt) and reacts with e$^-$ to form the Cu nuclei. The change

of current density favored the Cu_{aq}^{2+} outer Helmholtz plane (OHP) of electrical double layer to deposit on Pt electrode for overcoming the Gibbs free energy in region I. Subsequently, in region II as shown in figure, the constant current influence the Cu nanowire growth in the PAMs nano-channel in nearly steady-state diffusion of Cu_{aq}^{2+}. The current increment was observed in Region III due to the Cu nanowire approaching the PAMs surface and growth of the hemispherical caps at the ends of each nanowire. An outstanding region in the first step is shown in Fig. 4B, in which a smooth current density at 20-30 and 70-90 nm and a rapid change current density at 90-100 nm were observed. There are two possible factors influences the growth of single crystals in the electrochemical deposition process:

(i) The homogeneous current density distributes over the cathode surface [30].

(ii) For hemispherical nanowire structure, the relationship between current density (J) and nucleus radius (r_o) can be described as:

$$J=(zFDc)/r_o \qquad (1)$$
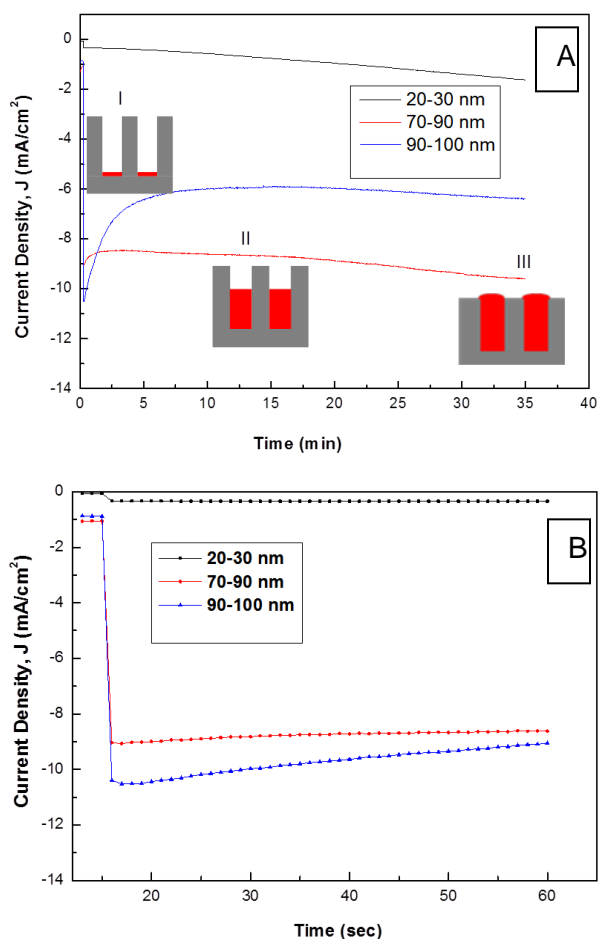
Fig. 4 (a, b) Sketch of J-t curve of Cu growth in various PAM pore sizes under a constant potential of -0.18 V/SCE.

Where z is the amount of electrons transferred in the reaction (z=2), F is Faraday's constant (96485.3 C mol^{-1}), D is the diffusion coefficient, and c is the concentration of the electrolyte [31, 32]. Based on the distribution of current density, different nanowire structures are formed.

In the case of 20-30 nm and 70-90 nm assisted Cu nanowires; the variety of current density was smooth, which demonstrated the homogeneous behavior over the cathode surface. Additionally, by comparing the initial current density in various pore size assisted Cu nanowire growth, it is observed that the current density increases gradually with an increase in pore size. This result also implies that the nucleus radius decreases gradually with an increasing pore size, which influences the nano-crystallite size [33]. Thus, the crystallinity of 20-30 nm and 70-90 nm nanowires is single crystalline in nature. However, when increasing the pore size to 90-100 nm, the mechanism of nanowire growth is attributed to the agglomeration of Cu particles. The fibrillar structure observed in the 90-100 nm nanowire was due to the rapid growth as the nano crystallite did not have enough time to undergo nucleation. When the nanowire was fabricated over to be 90 nm in size, the nanowire was found to be polycrystalline. Xu et. al [27] also reported that single crystal nanowire growth was achieved via atom-by-atom assembly of individual crystallites instead of the agglomeration of particles formed in the solution phase, which is very similar to our work.

The above results indicated that ordered Cu/PAMs nanowire arrays were synthesized, the crystallinity of which was varied by controlling the PAM pore size. **Fig. 5** shows the SEM images of the Cu$_2$O nanowire arrays with various diameters obtained after annealing the Cu nanowire arrays at 400°C for 8 h. Initially, the arrays were prepared inside PAMs and then became free standing after dissolving the PAMs by 1M NaOH for 30 min. Consequently, the size and shape of the nanowires correspond with the PAMs configuration. To confirm the composition of copper oxide, EDX measurement was carried out and, with **Fig. 5 (D)** offering the EDX analysis of the nanowire. Al and Ni elements were found due to the alumina template and Ni grid, respectively. EDX results indicate that the ratio between Cu and O is 2:1, which implies that the nanowires are indeed Cu$_2$O.
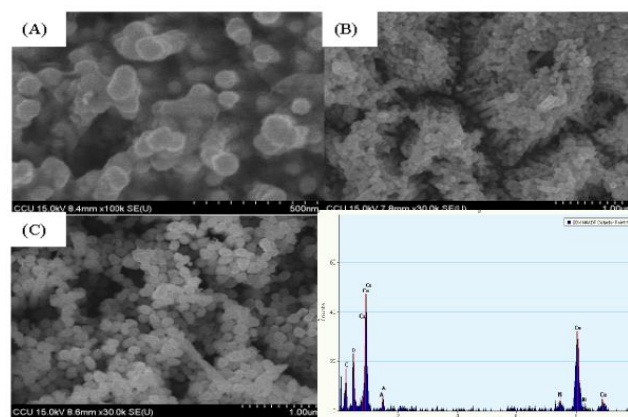
Fig. 5. Plane-view SEM images of Cu$_2$O nanowire arrays prepared within various pore sizes of PAMs (A) 20~30, (B) 70~90 and (C) 90~100a and (D) EDX analysis image of Cu$_2$O nanowire. The PAMs were removed using 1 M NaOH solution for 30 min.
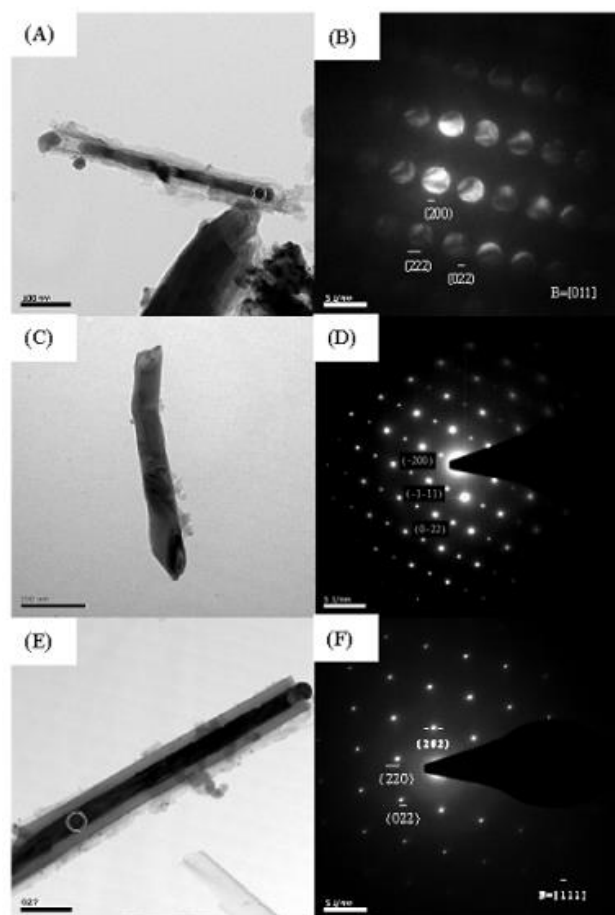
Fig. 6. TEM and ED images of Cu$_2$O nanowire arrays prepared within various PAM pore sizes (A, B) 20~30, (C, D) 70~90 and (E, F) 90~100 nm.

The crystallinity of individual nanowires was investigated from TEM and convergent beam electron diffraction (CBED) and select area electron diffraction (SAED) images as shown in **Fig. 6**. Compared to the SEM results, the TEM morphologies also implied the same results, with individual nanowire sizes were 20~30, 70~90 and 90~100nm. In addition, the observation of shell layer covered on the Cu$_2$O nanowire shown in **Fig. 6E** was remaining Al$_2$O$_3$, which was removed incompletely. The crystallinity of different size nanowires can be observed from the ED images. It was found that single crystals were synthesized for nanowire size of 20~30, 70~90, and 90~100 nm. The electron diffraction patterns of (200), (220), and (002) were observed in each single crystal nanowire (Figs. 6B, D, F); also, the d-spacing's d$_{(200)}$, d$_{(220)}$, and d$_{(002)}$ were found to be 2.06, 2.4, and 1.5 Å, respectively. Combined with the EDX analysis, the ED results also demonstrate the formation of FCC-Cu$_2$O during the heat treatment of Cu. In addition, the d-spacing in different diameters of single crystal nanowires were 2.39, 2.38, and 2.41 Å. The results also imply that the Cu$_2$O growth direction was (111) **[34].** In comparison to the synthesis of Cu nanowire, here, the O$_2$ atoms were diffused into the tetrahedral site of FCC-Cu during the heat treatment process to form Cu$_2$O. We can observe that the crystallinity was improved during the oxidation process and we can easily get the single crystal

Cu$_2$O. The results further imply that not only did the O$_2$ atoms diffuse into the Cu structure during heat treatment, but the Cu and O$_2$ lattice sites may also rearranged during the formation of nanowires. Cu$_2$O crystallizes in the cuprite structure where inside the unit cell the oxygen ions are located on a bcc sub-lattice, while copper ions on a fcc sub-lattice. The structure is favourable as it consists of two linkages of tetrahedral rotated 90^0 to each other and grows in preferential direction. During oxidation, atoms have sufficient energy to move to the correct lattice position, and crystalline grains are produced because of the low surface energy **[35]**. The major contribution to the oxidation reaction comes from lattice oxygen **[36].** Therefore, the oxygen mobility in the crystal lattice determines the crystallinity of nanowires due to changes in the periodicity of the materials **[37]**. The possible control of the oxidation behavior of Cu leads to artificial structural modifications of the oxide nanostructures **[38].** Based on above results, we can synthesize the appropriate Cu and/or Cu$_2$O single crystal nanowires using PAM for future electronic device applications. A comparison of this work and reported literature work for growth of Cu/Cu$_2$O nanowires is given in **Table 1** for better understanding. Our grown nanowires have been shown to be advantageous than the other work for possible application.

Table 1. Comparison of the present work on PAM with Cu/Cu$_2$O nanowires.

Nanostructure materials	Growth process	References
Polycrystalline Cu$_2$O	Electrochemical in aluminum template	Ko et al [39]
Polycrystalline Cu/Cu$_2$O	AC current electrochemical	Wang etal [34]
Cu nanowires	Chemical Vapour deposition	Choi et al [23]
Cu nanowires	Heat treatment	Yao et al [19]
Cu/Cu$_2$O composites nanowires	Aniodic aluminum template mediated electrodeposition	Lee etal [29]
Cu nanowires	Electrodeposition	Meier et al [11]
Cu$_2$O nanowires	Oxidation of Cu nanowires-Microwave irradiation	Nunes et al [21]
Cu and/ or Cu$_2$O single crystal nanowires	Electrochemical process with control pore size of PAM/ annealing in oxygen atmosphere	This work

Conclusion

We have successfully prepared various ordered pore sizes of PAMs by controlling the H$_2$SO$_4$ and H$_2$C$_2$O$_4$ electrolytes. Pore sizes are found to be 20~30, 70~90 and 90~100 nm by increasing the anodization voltage from 18 to 60 V. The crystallinity of Cu nanowire is influenced by various pore sizes of PAMs, such as single crystal behavior at 20 to 90 nm, and polycrystalline at 90~100 nm. The slow diffusion of Cu_{aq}^{2+} to the electrode surface caused the atom-by-atom agglomeration and thereby induced the single crystal behavior for nanowire sizes of less than 90 nm. The O$_2$ is diffused into the Cu lattice during the heat treatment, and the template space limitation induced the formation of Cu$_2$O phase. Moreover, the crystallinity is also improved in each condition due to the rearrangement of Cu and O$_2$ lattice

sites. The grown single crystal Cu and/or Cu_2O nanowire may play important role for the nano and optoelectronics devices.

References

1. Riveros, G.; Green, S.; Cortes, A.; Gomez, H.; Marotti, R. E.; Dalchiele, E. A.; Nanotechnology, **2006**, 17, 561.
   DOI: 10.1088/0957-4484/17/2/037
2. Wu, Y.; Yan, H.; Yang, p.; Chem. Eur. J. **2002**, 8, 1260.
   DOI: 10.1002/1521-3765(20020315)8:6<1260:: AID-CHEM1260>3.0.CO;2-Q
3. Mehmood,T.; Mukhtar, A.; Khan, B.; Wu, K.; American Journal of Chem. Engg., **2016**, 4(2), 57.
   DOI: 10.11648/j.ajche.20160402.15
4. Terris, B. D.; Thomson, T.; J. Phys. D: Appl. Phys., **2005**, 38, R199.
   DOI: http://dx.doi.org/10.1088/0022-3727/38/12/R01
5. Masuda, H.; Fukuda, K., Science **1995,** 9, 1466.
   DOI: 10.1126/science.268.5216.1466
6. Huczko, A.; Appl. Phys. A., **2000**, 70, 365.
   DOI: 10.1007/s003390051050
7. Martin, C. R.; Chem. Mater. **, 1996**, 8, 1739.
   DOI: 10.1021/cm960166s
8. Dellis, S.; Christoulaki, A.; Spiliopoulos, N.; Anastassopoulos, D. L.; Vradis, A. A.; J. Appl. Phys. **2013,** 114, 164308**.**
   DOI: http://dx.doi.org/10.1063/1.482690
9. Thompson, G. E.; Wood, G. C.; Nature **1981**, 19, 230.
   DOI: 10.1038/290230a0
10. Inguanta, R.; Piazza, S.; Sunseri, S.; Appl. Surf. Sci.,**2009**, 255, 8816.
    DOI: http://dx.doi.org/10.1016/j.apsusc.2009.06.062
11. Meier, L. A.; Alvarez, A. E.; Garcia, S. G.; delBarrio, M. C.; Procedia Mater. Sci., **2015**, 8, 617.
    DOI: 10.1016/j.mspro.2015.04.116
12. Napolskii, K. S.; Roslyakov, I. V.; Eliseev, A. A.; Petukhov, D. I.; Lukashin, A. V.; Chen, S. F.; Liu, C. P.; Tsirlina, G. A.; Electrochimica, **2011**, 56, 2378.
    DOI:http://dx.doi.org/10.1016/j.electacta.2010.12.013
13. Inguanta, R.; Piazza, S.; Sunseri, C.; Nanotechnology, **2007**, 18, 485605.
    DOI:http://dx.doi.org/10.1088/0957-4484/18/48/485605
14. Chik, H.; Liang, J.; Cloutier, S. G., Kouklin, N.; Xu, J. M.; Appl. Phys. Lett., **2004**, 84, 3376.
    DOI: http://dx.doi.org/10.1063/1.1728298
15. Zhou, H.; Wong, S. S.; ACS Nano, **2008**, 2**,** 944
    DOI: 10.1021/nn700428x
16. Tan, M.; Chen, X.; Journal of the Electrochemical Society, **2012,** 159, K15
    DOI*:10.1149/2.034201jes*
17. Shen, Y. M.; Pan, C. H.; Wang, S. C.; Huang, J. L.; Thin Solid Films, **2011**, 520,1532.
    DOI: http://dx.doi.org/10.1016/j.tsf.2011.09.066
18. Han, U. B.; Lee, J. S.; Scientific Reports**, 2016**, 6, 25537**.**
    DOI: 10.1038/srep25537
19. Yao, Z.; Lu, Y. W.; Kandlikar, S. G.; Micro and Nano Letters, **2011,** 6, 563
    DOI: 10.1049/mnl.2011.0136
20. MacDonald, A. M.; Nature, **2001**, 414, 409.
    DOI : 10.1038/35106685
21. Nunes, D.; Pimentel, A.; Barquinha, P.; Carvalho, P. A.; Fortunato, E.; Martins, R.; Microsc. Microanal **2015,** 21, 112**.**
    DOI: 10.1017/S1431927614014263
22. Oh, J.; Tak, Y.; Lee, J.; Electrochem. Solid-State Lett., **2004**, 7, C27.
    DOI*: dx.doi.org/10.1149/1.1642575*
23. Choi, J. S.; Ko, E. S.; Kang, J. K.; Tak, Y. S.; Lee, J.; J. Ind. Eng. Chem., **2007**, 13, 305.
    DOI: not available
24. Inguanta, R.; Sunseri, C.; Piazza, S.; Electrochem. Solid State Lett., **2007**, 10, K63.
    DOI: 10.1149/1.2789403
25. Inguanta, R.; Piazza, S.; Sunseri, C.; Electrochim. Acta, **2008**, 53, 6504.
    DOI: http://dx.doi.org/10.1016/j.electacta.2008.04.075
26. Liu, B.; Aydil, E. S.; J. Am. Chem. Soc., **2009**, 131, 3985.
    DOI: 10.1021/ja8078972
27. Xu, D. S.; Xu, Y. J.; Chen, D. P.; Guo, G. L.; Gui, L. L.; Tang, Y. Q.; Adv. Mater. **2000,**12, 520.
    DOI: 10.1002/(SICI)1521-4095(200004)12:7<520:: AID-ADMA520>3.0.CO;2-#
28. Shen, Y. M.; Shih, Y. T.; Wang, S. C.; Nayak, P. K.; Huang, J. L.; Thin Solid Films **2010**, 519, 1687.
    DOI:http://dx.doi.org/10.1016/j.tsf.2010.08.087
29. Lee, W.; Ji, R.; Osele, U.; Nielsch, K.; Nature Materials, **2006**, 5, 741.
    DOI: 10.1038/nmat1717
30. Dobrev, D.; Vetter, J.; Angert, N.; Neumann, R.; Appl. Phys. A **1999**, 69, 233.
    DOI: 10.1007/s003390050995
31. Delahay, P.; New Instrumental Methods in Electrochemistry, Inter science, New York, **1954**.
    DOI: 10.1002/bbpc.19560600517
32. Gunawardena, G.; Hills, G.; Montenegro, I.; Scharifker, B.; J. Electroanal. Chem.,**1982**, 138, 225.
    DOI: 10.1016/0022-0728(82)85080-8
33. Ghahremaninezhad, A.; Dolati, A.; ECS Transactions, **2010,** 28, 13.
    DOI: 10.1149/1.3503348
34. Wang, X.; Li, C.; Chen, G.; He, L.; Cao, H.; Zhang, B., Solid State Sci., **2011**, 13, 280.
    DOI: 10.1016/j.solidstatessciences.2010.11.005
35. Wang, H. C.; iao, C. H.; Chueh, Y. L.; Lai,C. C.; Chou, P. C.; Ting S. Y.; Optical Mater. Exp. 2013, 3, 295
    DOI: https://doi.org/10.1364/OME.3.000295
36. Grenier, J.C.; Schiffmacher, G.; Caro, P.; Pou Hagenmuller P.; Chard, M.; Hagenmuller, P.; J. Solid State Chem. **1977**, 20. 365-379
    DOI: http://dx.doi.org/10.1016/0022-4596(77)90174-8
37. Fierro, J. L. G. (Eds); Metal oxides: Chemistry and Applications, CRC press, Taylor & Francis Group 2006,p550
    DOI: Fierro/p/book/9780824723712#
38. Cai, S. M.; Matsushita, T.; Fujii, H.; Shirai, K.; Nonomura, T.; Tatsuoka, H.; Hsu, C. W.; Wu, Y. J.; Chou, L. J.; e-J. Surf. Sci. Nanotech. **2012**, 10, 175.
    DOI: http://doi.org/10.1380/ejssnt.2012.175
39. Ko, E.; Choi, J.; Okamoto,K.;Tak, Y.; Lee, J.; Chem. Phys. Chem, **2006** , 7, 1505
    DOI: 10.1002/cphc.200600060